Natural Hazards
https://doi.org/10.1007/s11069-024-07052-8

ORIGINAL PAPER

Analysis of the forest fire in the 'Bohemian Switzerland' National Park using Landsat-8 and Sentinel-5P in Google Earth Engine

Furkan Yilgan[1] · Markéta Mihálikova[1] · Recep Serdar Kara[1] · Mustafa Ustuner[2]

Received: 17 July 2023 / Accepted: 22 November 2024

Abstract
The recent increase of the air temperature due to the global climate change is considered as one of the important reasons for the wildfires increase in the world, even in areas where the wildfires are not that common. In addition to the various physical damages adversely affecting the ecological balance, harmful gases and solid particles are released into the atmosphere due to wildfires, causing serious health problems. In this study, impacts of the most serious forest fire in modern history of the country lasting 16 days from 23rd of July 2022 in the National Park" *Bohemian Switzerland*" in the Děčín district, Czech Republic, were investigated using remote sensing satellite datasets by cloud-based Google Earth Engine (GEE) platform. The normalized difference moisture index (NDMI), normalized burn ratio index (NBR), normalized difference vegetation index (NDVI), land surface temperature (LST) and soil moisture index (SMI) were calculated from Landsat-8 Operational Land Imager and Thermal Infrared Sensor (OLI and TIRS) dataset for the dates of 31st October 2021, 18th June 2022, and 31st October 2022. Relationship of the remote sensing indices were calculated to estimate the impacts of the wildfire. Furthermore, distribution of nitrogen dioxide (NO_2) was extracted using Sentinel-5P TROPOMI (Tropospheric Monitoring Instrument) to observe changes before and after the forest fire in the study region. The burnt area approximately 13.20 km^2 from the total area of 79.28 km^2 was detected using different time series of the remote sensing indices in the national park.

Keywords Climate change · Environmental disaster · Land surface temperature · Remote sensing · Wildfires

1 Introduction

Forest fires occur from the past to the present in the world and some of the fires are caused by human effects while some of them are caused by harsh climatic conditions (Mansoor et al. 2022). Climate change is considered as one of the most important causes of natural fires

Extended author information available on the last page of the article

due to the extreme climate conditions and rising average temperature all over the world that trigger global warming and increase the risk of wildfires (Lohmander et al. 2022). Increasing population density, greenhouse gases and industrialization activities are the main reasons of the global warming in the world (Al-Ghussain 2019). As a consequence, wildfires lead to the deterioration of the structure of nature. Additionally, apart from the climatic conditions, the rapid urbanization of megacities also disrupts the natural ecosystems' structure and leads to the conversion of agricultural areas and forests into settlements. Moreover, many natural disasters affect landscape structure and environment, such as earthquakes, wildfires, and landslides, which change the characteristics of the Earth surface (Ishtiaque and Nazem 2017). Therefore, the devastation of agricultural lands and forest areas not only contributes to a rise in air temperature but also precipitates significant global environmental transformations. Additionally, it inflicts harm upon ecosystems and disrupts organic cycles within habitats, as highlighted by Xiuwan (2002). Wildfires also cause soil erosion and land degradation which worsens the structure of the soil and makes it less suitable for sustainable farming (Depountis et al. 2020). The diversity of species is highly affected by wildfires due to the destruction of the habitats (McLauchlan et al. 2020; Walter et al. 2022). Thus, the environment is an important factor for the survival and ecological cycles of species are seriously affected by changes in the environment due to wildfires. Apart from all these, air quality deteriorates as high concentrations of dangerous gases and atmospheric particulate matter are released into the atmosphere due to forest fires (Bo et al. 2020). Thus, these harmful gases and particulates easily enter to human body through the respiratory system and causing diseases such as acute or chronic asthma, hearth attack and serious lung diseases. For these reasons, it is very important to quickly examine effects of the forest fires and determine the damage they cause to the environment.

With the development of high-resolution sensors, unmanned aerial vehicle systems (UAV) and remote sensing satellite data have become commonly used tools examining forest fires and other natural disasters. These technologies are highly beneficial as they can swiftly collect data across different wavelengths of the electromagnetic spectrum. This allows rapid evaluation of natural disaster management strategies and subsequent assessment of damage inflicted upon nature. Moreover, the effects of wildfires and forest fires can be observed using remote sensing satellite data by calculating different temperature and moisture indices.

Land surface temperature (LST) and soil moisture index (SMI) play important roles in climate studies, and these indices can be calculated using remote sensing satellite systems as much as reliable in situ measurements. Normalized burn ratio index (NBR), normalized difference moisture index (NDMI) and normalized difference vegetation index (NDVI) are effectively used to obtain information about vegetation density and discriminate burnt areas because vegetation absorb the sunlight due to photosynthetic activity and extra absorbed energy is emitted to the atmosphere. Therefore, near infrared and shortwave infrared bands of the satellite have an ability to observe the emitted energy from objects such as vegetation and soil.

Furthermore, the risk assessment of forest fires can be conducted by monitoring meteorological drought using remote sensing data enabling detection before wildfires occur (Bentchakal et al. 2022). The air quality and surface temperature values of a region are related to land use and land cover types as well as climate variables of the region, such as wind and precipitation (Yin et al. 2020). The measurement of the air pollution ratio in a small region may be possible using ground stations but remote sensing technology is highly useful for monitoring large areas in the world.

One of the most significant pollutants in the air is nitrogen dioxide (NO_2), which can be observed by measuring its concentration using remote sensing data provided by Sentinel-5P TROPOMI (Tropospheric Monitoring Instrument) (Rabiei-Dastjerdi et al. 2022). During and after wildfires, the concentration of NO_2 in the atmosphere can significantly increase, i.e. due to the combustion of organic matter, such as nitrogen in the organic horizons and plant material (Keeley and Fotheringham 1997). High temperatures during fires cause these materials to oxidize, forming NO_2 and other nitrogen oxides (NO_x). This NO_2 can undergo further transformations in the atmosphere: photochemical reactions may revert it back into nitrogen and oxygen, or it may interact with volatile organic compounds (VOCs) under sunlight to form ozone (Leighton 2012). The fate of NO_2 also depends on atmospheric dispersion, influenced by factors like wind patterns, topography, and weather, leading to its deposition back onto the land, absorption by water bodies, or long-distance travel (Adams et al. 2019). These changes in NO_2 and other pollutants post-wildfires can adversely affect air quality and human health, as reported by Naqvi et al. (2023). Their study reveals an overlap of increased pollutant levels with rising mortality in Covid-19 cases. Evaluating changes in NO_2 concentration following wildfires is vital for maintaining air quality, safeguarding environmental health, addressing climate change, guiding public health planning, and informing policy development.

The Bohemian Switzerland National Park is one of the important tourist destinations in the Czech Republic, it is a unique sandstone area that is habitat of many rare animals and plants, and the unique biodiversity is primarily a reflection of the diversity of the geological formation. The national park is visited by many tourists throughout the year due to its natural beauty; the most attractive is the largest rock arch of natural origin in Europe. The Bohemian Switzerland National Park due to its geological origin is under risk of wildfires and actually various forest fires occurred in the past such as wildfire on 22nd July 2006. However, huge forest fires rarely occur in the Czech Republic as it belongs to the temperate climatic zone. The biggest fire in modern Czech history so far started on 23rd of July in 2022 in this national park. It took almost 16 days to extinguish on the Czech side, and 23 days on the German side, because the fire spread across the country border to the Saxon Switzerland National Park. Forest fires were investigated by examining the data of past fires between 1997 and 2019 in the Czech Republic, and the study shows that fires occur more frequently in the region where the national park is located (Špulák 2022). Furthermore, historical investigations of forest fires between 1992 and 2004 have shown that forest fires occurred mainly in April and August in the Czech Republic (Kula and Jankovská 2013). In addition, according to annual report of European Forest Fire Information System (EFFIS) in 2021, 1517 forest fires were recorded in 2021 and approximately 411 ha of forests were burned in the Czech Republic (San-Miguel-Ayanz et al. 2022). This is reported as one of the most severe fire seasons in the last 20 years. For a better insight, 10 years average is 375 ha of burnt forest area in the country. As expected, an increased value of burnt area was reported in 2022, amounting to 1438 ha, of which 1062 ha comprised coniferous forest (San-Miguel-Ayanz et al. 2023). Forest fires can be caused by human activity or by natural changes such as high temperatures. However, forest fires, especially in the Czech Republic, are typically associated with human influence, often from residents of surrounding areas or tourists camping in the forests (Berčák et al., 2022). In spring 2023 was arrested the offender, who started this particular fire in the national park on purpose during the period of drought (as can be found in local media).

There are several studies held for examining the impacts of forest fires with optical and radar remote sensing data. Impacts of forest fire on climate and land cover changes was analysed by De Jesus et al. (2022) and degraded soil areas were observed using remote sensing indices. Changes of land use and land cover types were investigated by Trochta et al. (2012) after the forest fire in 2006 for the Bohemian Switzerland National Park using remote sensing data by applying a supervised classification method and found the fire severity on the ground and in the canopy which had a strong correlation between each other. Sannigrahi et al. (2020) explored different vegetation indices such as NBR, NDMI and LST using Moderate Resolution Imaging Spectrometer (MODIS) remote sensing data to observe effects of forest fire in India and the study showed that the moisture indices are found to be the most suitable and spatially coherent burn indicators between the burn indices. Lambin et al. (2003) used NDVI and LST to estimate the burn efficiency of forest fires for different seasons in the Central Africa and results showed successfully that temperature values were highest and NDVI values were lowest after the forest fire. In addition, several remote sensing indices were used by Chung et al. (2019) for the estimation of burnt areas using threshold techniques after forest fire such as NDVI and NBR and the study demonstrated that the accuracy assessment of damage will be improved with near-daily monitoring of Earth surface. Yuan et al. (2017) observed a wildfire and evaluated the resulting damage using multispectral and hyperspectral sensors by UAV systems and the results verified that the designed method can effectively extract the fire pixels. Medvedkov et al. (2023) analysed the relationships between remote sensing indices, such as vegetation, moisture, and surface temperature, to detect geocryological conditions in forest areas and they found that on maps displaying LST, the ranges of these natural ecosystems become apparent as conspicuous "thermal islands," where the intensity of colour corresponds to the extent of permafrost's influence on forest growth conditions.

Most of the wildfire research was conducted in the regions like North America, Australia, and Southern Europe, where wildfires are more common than in Central European regions such as the Czech Republic. However, this is still a challenging and complicated process to understand the spreading and consequences of the wildfire because each particular region has different ecological characteristics (i.e. region-specific wildfires). Kudláčková et al. (2024) investigated different scenarios of this fire conditions, propagation, and extent and how these fire behavior characteristics could be affected e.g. by forest management. The report of Hruška et al. (2022) focused mainly on factors affecting the origin and spread of the fire. Despite these advancements, there remains a significant gap in comparison pre- and post-fire conditions in Bohemian Switzerland National Park, and no remote sensing study has been published to the present knowledge of the authors. Hence, such overall summary is crucial for the preservation of natural heritage as well as to characterize and understand the region-specific wildfires. Additionally, while remote sensing is widely used in post-fire analysis, the integration of multiple indices and the use of cloud-based platforms like Google Earth Engine for such comprehensive analysis is still emerging.

The aim of the current study is the early detection of the changes in vegetation, air quality and temperature after a forest fire in the national park "Bohemian Switzerland" using remote sensing methods in the Czech Republic because this catastrophe seriously affected public life of inhabitants in the Czech Republic and to our best knowledge, the spreading and emission of the harmful gases has not been thoroughly investigated by remote sensing method so far. The vegetation density and land surface temperatures were calculated and the relationship between them were examined before and after the forest fire. Moreover, water content of the plants and soil moisture were investigated to analyse their relationship between vegetation density and surface temperature. The relationship of temperature changes with soil moisture and vegetation provides clear ideas about the effects of forest fire in the region before and after the event. Estimation of the burned area will be calculated using NBR and NDVI indices before and after the forest fire. The effects of forest fires on air quality will be examined by analysing the change of the NO_2 ratio in the air.

2 Materials and methods

2.1 Study area

The main study area was chosen in the northwest part of the Czech Republic, located approximately between latitudes 49° and 51° N and longitudes 13° and 16° E. It covers the Bohemian Switzerland National Park and the adjacent regions in the direction of prevailing winds. The climate of the Czech Republic is defined by the interweaving and mixing of oceanic and continental influences (Skalák et al. 2018). The main study area consists of Děčín, Česká Lípa and Mladá Boleslav districts and is shown in Fig. 1. This area covers 3002.61 km^2, which represents 3.8% of the total area in the Czech Republic. The Bohemian Switzerland National Park where forest fires occurred is shown in Fig. 1. It is located in Ústecký Kraj region and covers totally area of 79.28 km^2. Approximately half of the park area is covered by forest ecosystems, mostly coniferous. Long-term annual average of the precipitation and temperature in the region are 636 mm and 8.2 °C, respectively. The summer of 2022 was 2.7 °C warmer in this region than the long-term average of 1961–2000 (Hruška et al. 2022).

2.2 Datasets

Landsat-8 OLI (Operational Land Imager) and TIRS (Thermal Infrared Sensor) and Sentinel-5P TROPOMI images were used as input datasets. Landsat-8 surface reflectance (Level-1) data have 30 m spatial resolution and 11 different spectral bands. The temporal resolution of the satellite is 16 days, and the satellite has two thermal bands which have 100 m spatial resolution.

The Landsat-8 raw and surface reflectance datasets were obtained using Google Earth Engine (GEE) cloud-based platform for the dates 31st October 2021, 18th June 2022, and 31st October 2022. Landsat-8 images were filtered as coverage of less than 20% of the clouds and raw satellite images are shown in Fig. 2.

Sentinel-5P TROPOMI is a spectrometer that has 7 km × 3.5 km spatial resolution and can detect different wavelengths such as ultraviolet (UV), visible (VIS), near (NIR), and short-wavelength infrared (SWIR) to monitor ozone, methane, formaldehyde, aerosol, carbon monoxide, nitrogen dioxide, and sulphur dioxide in the atmosphere. Offline high-resolution imagery of NO_2 concentrations is obtained from Sentinel-5P TROPOMI satellite by using GEE platform. The related data were gathered for the days between July 19th and

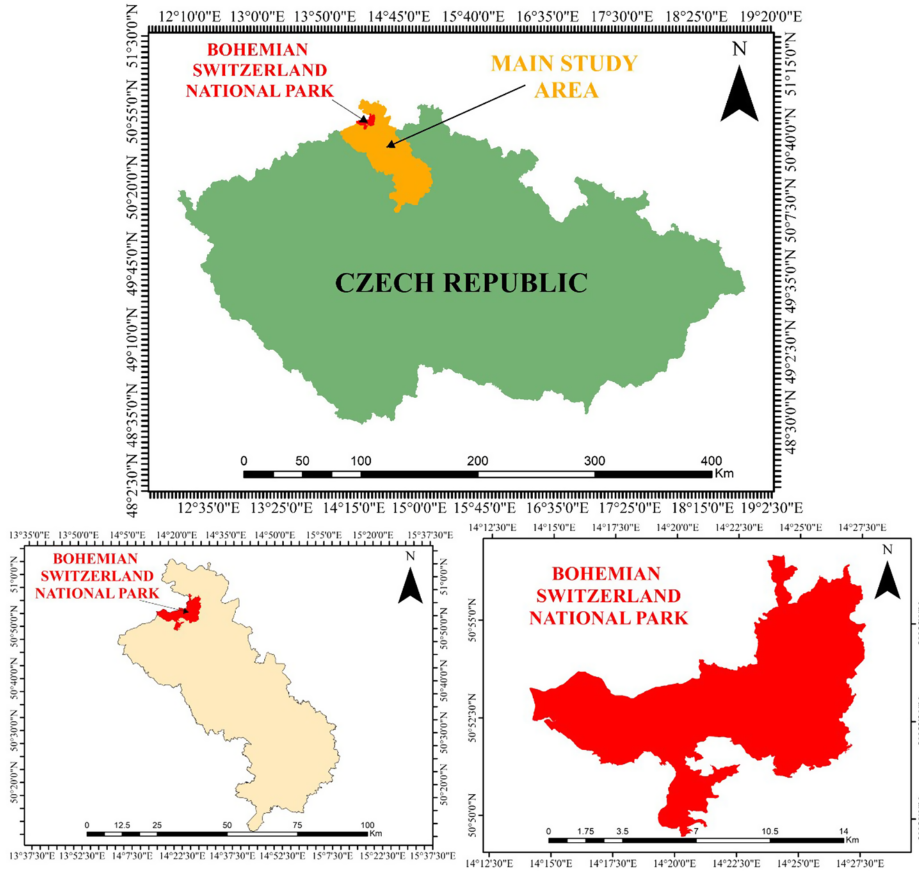

Fig. 1 The Bohemian Switzerland National Park and the main study area in the Czech Republic

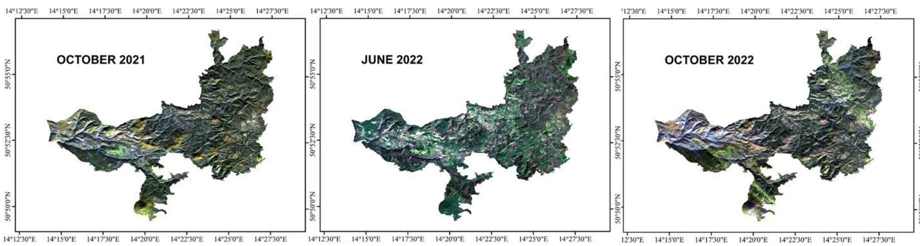

Fig. 2 Raw Landsat-8 satellite images of the Bohemian Switzerland National Park

July 21st, 2022, that is, before the forest fire, and then on August 21st to 23rd, 2022, that is, after the forest fire.

2.3 Methodology

Google Earth Engine (GEE) is a cloud-based platform that works based on JavaScript and Python programming languages that provides remote sensing satellite datasets to users (Gorelick et al. 2017). The processing of the images to observe the changes was performed using the GEE platform. The data for October had to be examined to conduct the research instead of August and September due to the temporal resolution of the Landsat-8 data and the cloudy weather conditions in the study area. The cloud mask and spatial mosaic were applied to the dataset using the GEE platform that can calculate the average values of the images in the related time range and can create a mosaic image from remote sensing dataset. The process of image preparation and calculated remote sensing indices are shown in Fig. 3 as a flowchart.

2.3.1 Normalized difference burn ratio index (NBR)

NBR is used to determine burned areas due to the difference between the reflectance of healthy vegetation and burned vegetation in the short-wave infrared interval of the electromagnetic spectrum (Tonbul et al. 2016). NBR is calculated using near infrared and short-wave infrared band of the satellite using formula that is given in Eq. (1) (Smith et al. 2005).

$$\mathrm{NBR} = (\mathrm{NIR} - \mathrm{SWIR}_2) / (\mathrm{NIR} + \mathrm{SWIR}_2) \tag{1}$$

Where NBR is the normalized burn ratio index, NIR is the near-infrared band of the satellite and $SWIR_2$ is the short-wave infrared band of the satellite that has 2.11–2.29 µm wavelength.

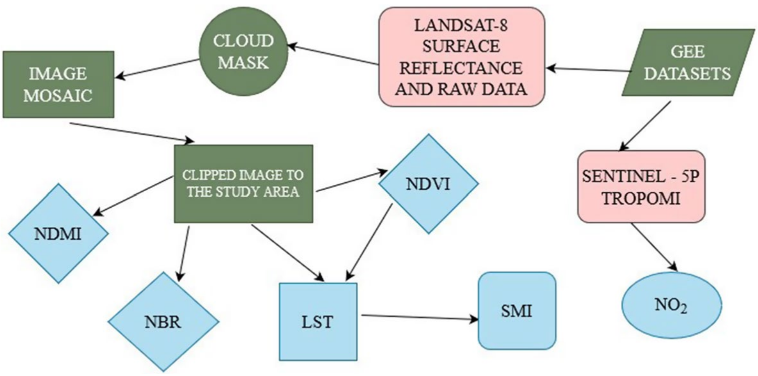

Fig. 3 Methodology of image processing and calculated remote sensing indices

2.3.2 Normalized difference moisture index (NDMI)

NDMI is a parameter that can show the water content of vegetation (Siachalou et al. 2009). NDMI is calculated using bands of surface reflectance data of Landsat-8 images. Near infrared and shortwave infrared values are used to calculate by formula that is given in Eq. (2) (Xu 2006).

$$\mathrm{NDMI} = (\mathrm{NIR} - \mathrm{SWIR}_1) / (\mathrm{NIR} + \mathrm{SWIR}_1) \tag{2}$$

Where SWIR_1 is a first shortwave infrared band of the satellite, and its wavelength is between 1.57 and 1.65 µm. NIR represents the near-infrared band of the satellite.

2.3.3 Normalized difference vegetation index (NDVI)

NDVI is the index that has a range between −1 and 1 and NDVI is mostly used to detect vegetation density. Values below 0 represent water, ice, and stones, while values between 0 and 0.2 are considered as pixels of bare soil. Values above 0.2 generally represent areas covered with vegetation, and closer to 1, the vegetation density increases. NDVI is calculated using the red and near infrared bands of Landsat-8 surface reflectance data with a formula given in Eq. (3) where NIR is the near infrared band, while R is the red band of the satellite (Tucker 1979).

$$\mathrm{NDVI} = (\mathrm{NIR} - \mathrm{R}) / (\mathrm{NIR} + \mathrm{R}) \tag{3}$$

2.3.4 Land surface emissivity (LSE)

LSE is a key parameter for the calculation of land surface temperature. Electromagnetic energy has some interactions with objects, and energy can be reflected, transmitted, and absorbed by objects. The absorbed energy is then slowly spread outward from the object, and this diffusion process can be detected with the help of thermal sensors. Every object has an emissivity value between 0 and 1. An object with an emissivity value of 1 is considered perfect reflective, while a substance that has 0 emissivity is considered blackbody (Weng et al. 2004). Under normal conditions, there is no perfect reflective material with an emissivity value of 1 in the world (Sobrino et al. 2004).

Land surface emissivity values are calculated by NDVI thresholding method, and this method considers NDVI values less than 0.2 to be bare soil, while those greater than 0.5 are considered vegetation. Pixels that are equal to or between 0.2 and 0.5 are defined as mixed pixels. While the bare soil emissivity value is considered as the reflectance values in the red band, the vegetation covered pixels are assigned an emissivity value of 0.99 and the emissivity of the mixed pixels is calculated using the formula given in Eq. (4) (Sobrino and Raissouni 2000).

$$\epsilon = \epsilon \mathrm{V}^{*}\mathrm{PV} + \epsilon \mathrm{S}^{*}(1 - \mathrm{PV}) + \mathrm{d}\epsilon \tag{4}$$

where ε is emissivity, εV represent emissivity of vegetation while εS is soil emissivity and PV is proportion of vegetation that calculates by using minimum and maximum NDVI values. PV is calculated by Eq. (5) using 0.2 and 0.5 for the minimum and maximum NDVI values.

$$\mathrm{PV} \;=\; ((\mathrm{NDVI} - \mathrm{NDVI}_{min}) \,/\, (\mathrm{NDVI}_{max} - \mathrm{NDVI}_{min}))^2 \tag{5}$$

dε is geometry factor of object and its formula is given in Eq. (6) where F is a constant that is considered as the shape factor of Earth topography and estimated value is calculated as 0.55 by Sobrino et al. (1990).

$$d\epsilon \;= (1 - \epsilon \mathrm{S}) * (1 - PV) * F * \epsilon \mathrm{V} \tag{6}$$

2.3.5 Brightness temperature of the satellite (B_T)

The brightness temperature of the satellite is found by conversion and calibration of the raw satellite datasets because raw data are stored as digital numbers which are not represented as a meaningful unit. Therefore, the raw pixels of the satellite images are converted to spectral radiance (TOA) values using the formula given in Eq. (7) (Ihlen 2019).

$$\mathrm{L}_\lambda \;=\; \mathrm{M}_L * \mathrm{Q}_{CAL} + \;\mathrm{A}_L \tag{7}$$

Where L_λ is spectral radiance values of satellite images, raw data band of the satellite is Q_{CAL}, A_L and M_L are stored in metadata information of satellite and M_L is a rescale factor of the satellite and A_L is additive rescaling factor. Brightness temperature values are calculated using thermal conversion constants K_1 and K_2, which are given in Eq. (8).

$$\mathrm{B}_T = \mathrm{K}_2 / \left(\ln \left(\mathrm{K}_1 / \mathrm{L}_\lambda \right) + 1 \right) \tag{8}$$

L_λ is the spectral radiance, B_T is the brightness temperature of the satellite in Kelvin (K) unit. According to thermodynamic experiments on the Kelvin temperature scale by Guildner and Edsinger (1973), 0 °C is accepted as equal to 273.15 K.

2.3.6 Land surface temperature (LST)

LST plays an important role for environmental studies and values of surface temperature can be calculated by different methods using thermal satellite data. LST is calculated using the emissivity and brightness temperature of the satellite parameters that are given in Eq. (9) (Dash et al. 2002).

$$\mathrm{LST} = \mathrm{B}_T / \left(1 + \left(\lambda * \mathrm{B}_T / \rho \right) * \ln \left(\epsilon \right) \right) \tag{9}$$

Where B_T is the brightness temperature of the satellite, λ is the mean wavelength of the emitted radiance and ρ is the blackbody law constant that is called Planck's constant. Flowchart of the calculation method is shown in Fig. 4 that shows two different data types of Landsat-8 satellite datasets. Top of atmosphere spectral radiance values were calculated using raw datasets while NDVI was calculated using surface reflectance dataset because

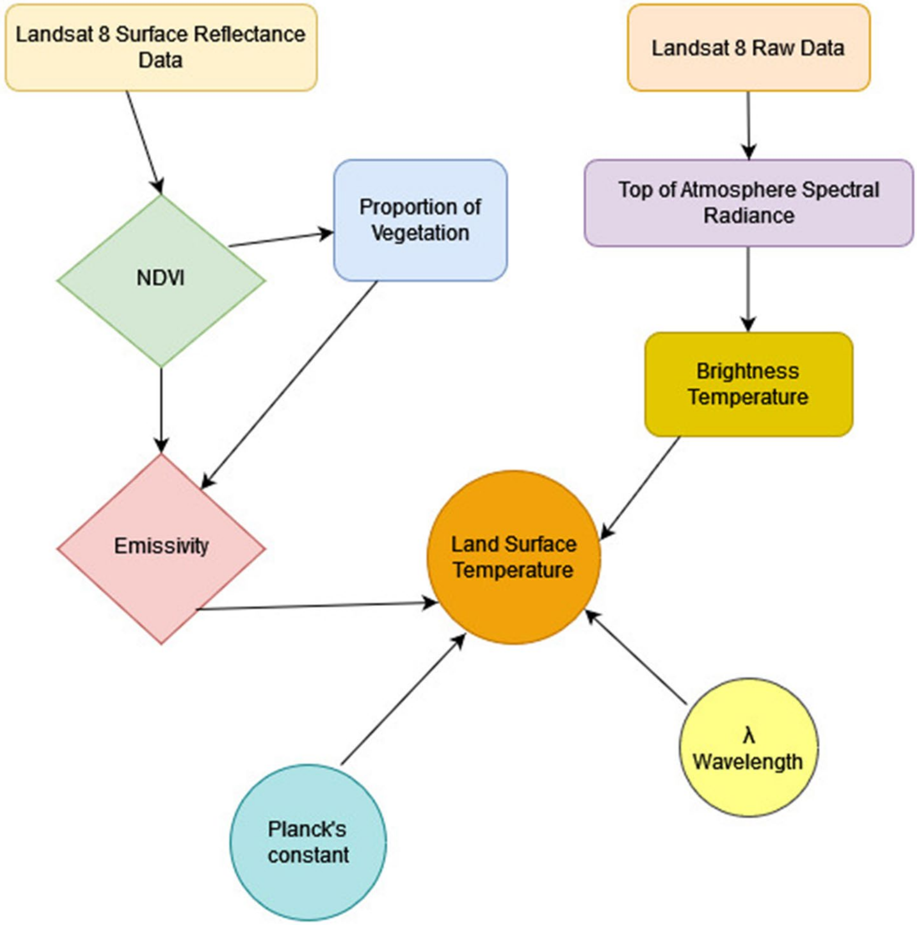

Fig. 4 Calculation method of land surface temperature

accuracy of surface reflectance datasets is higher than raw data. Thus, NDVI was obtained using surface reflectance datasets.

2.3.7 Soil moisture index (SMI)

The estimation of the soil moisture index is based on the maximum and minimum LST values shown in Eq. (10) where SMI is soil moisture index, LST is the land surface temperature layer that is calculated using Landsat-8 data and LST_{MAX}, and LST_{MIN} are the maximum and minimum values of the LST layers in the study area, respectively (Parida et al. 2008).

$$\mathrm{SMI} = (\mathrm{LST}_{MAX} - \mathrm{LST}) / (\mathrm{LST}_{MAX} - \mathrm{LST}_{MIN}) \tag{10}$$

2.3.8 Extraction of nitrogen dioxide gas

The concentrations of NO_2 gas (NO2_column_number_density) were extracted using GEE platform by Sentinel-5P TROPOMI satellite that was launched on 13 October 2017. Sentinel 5P TROPOMI has push broom scanner for observation of ultraviolet, visible, near infrared and shortwave infrared intervals of the electromagnetic spectrum (Gorelick et al. 2017). The mean of the pixel values was calculated and the average NO_2 maps before and after the forest fire in 2022 were created.

2.3.9 Accuracy assessment and statistical evaluation of the data

Accuracy assessment is applied using the Moderate Resolution Imaging Spectrometer (MODIS) data for the land surface temperature values. MODIS has daily temporal resolution and land surface temperature data are provided by the satellite every day. The spatial resolution of Landsat-8 LST data is resampled to 1 km MODIS daily data (MOD11A1) and 32 homogeneous points were used to achieve a correlation and root mean square deviation (RMSD) between the two datasets. Relationships between indices also were checked using 32 homogeneous correlation points, and scatterplots were created to show their statistical evaluations using Statistica v13 (TIBCO Software Inc., USA) software. The homogenous distribution of 32 points is shown in Fig. 5 in the study area.

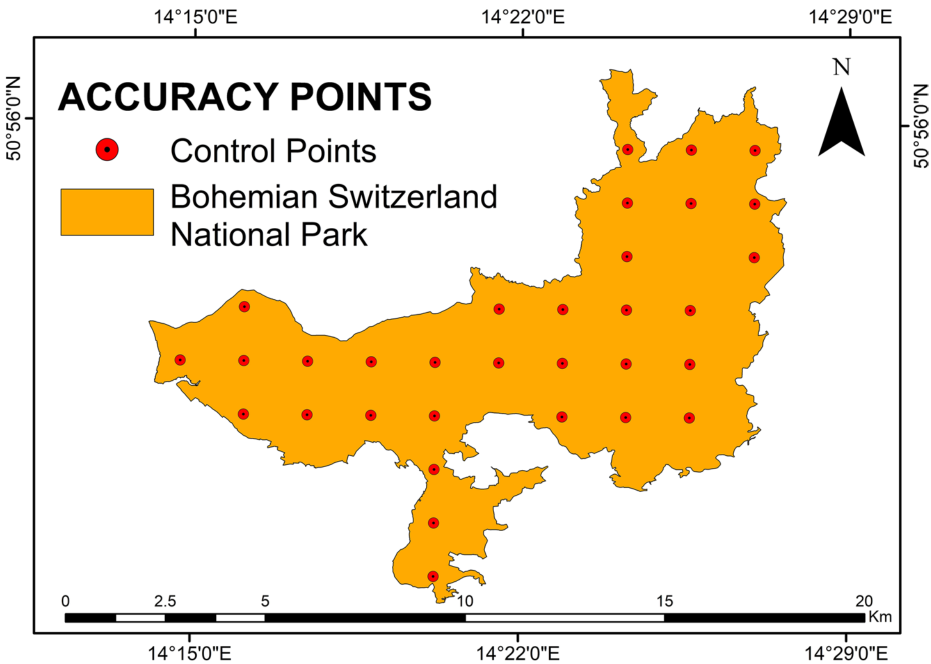

Fig. 5 Distribution map of the 32 homogeneous control points in the study area

3 Results

NDVI maps are shown in Fig. 6 which play a critical role to discriminate vegetation dense and bare soil from each other. According to NDVI maps, June 2022 has the highest vegetation cover, while October 2021 had more vegetation than October 2022. The NDMI maps shown in Fig. 6 showed that the lowest values of the moisture content of the plants are established in October 2022 in the study area. NDMI and NDVI indices can be useful to observe changes on vegetated areas due to near infrared and shortwave infrared ability of the satellite. In addition, the NDVI and NDMI maps show the vegetation change in the national park between the summer in June and autumn seasons in October 2021 and 2022. Both the NDMI and NDVI values showed a significant decrease after the wildfire in October 2022, compared to the same date in the previous year (October 2021). The decrease was

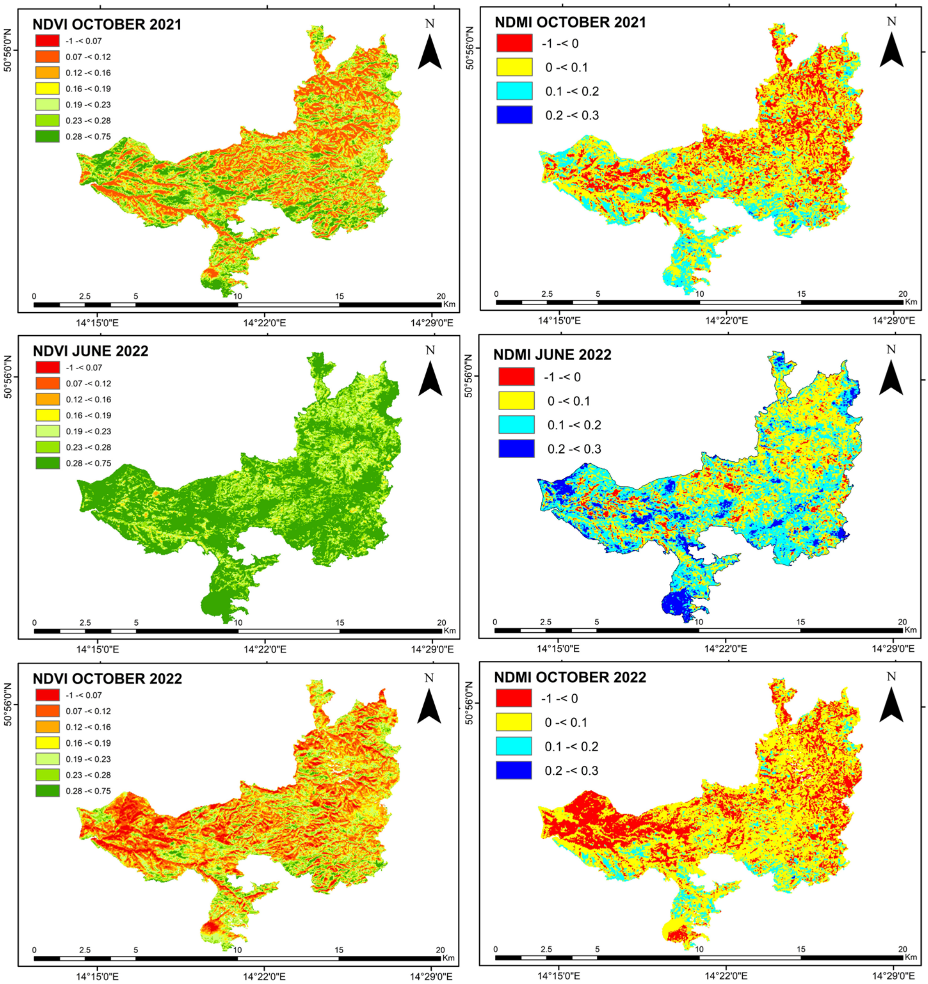

Fig. 6 NDVI (left) and NDMI (right) maps of the study area

more pronounced in the western part of the national park, which experienced the wildfire's high-intensity impact.

The maps of NBR are shown in Fig. 7 and areas affected by fire are discriminated by NBR as well as NDVI in October 2022. The change between summer and autumn months is observed in NBR maps as well as in NDVI and NDMI maps. On the October 2022 map, it is seen that the burned forest areas have NBR values below 0. When two different maps of the same month, dated 2021 and 2022, are taken into account, the vegetation destruction

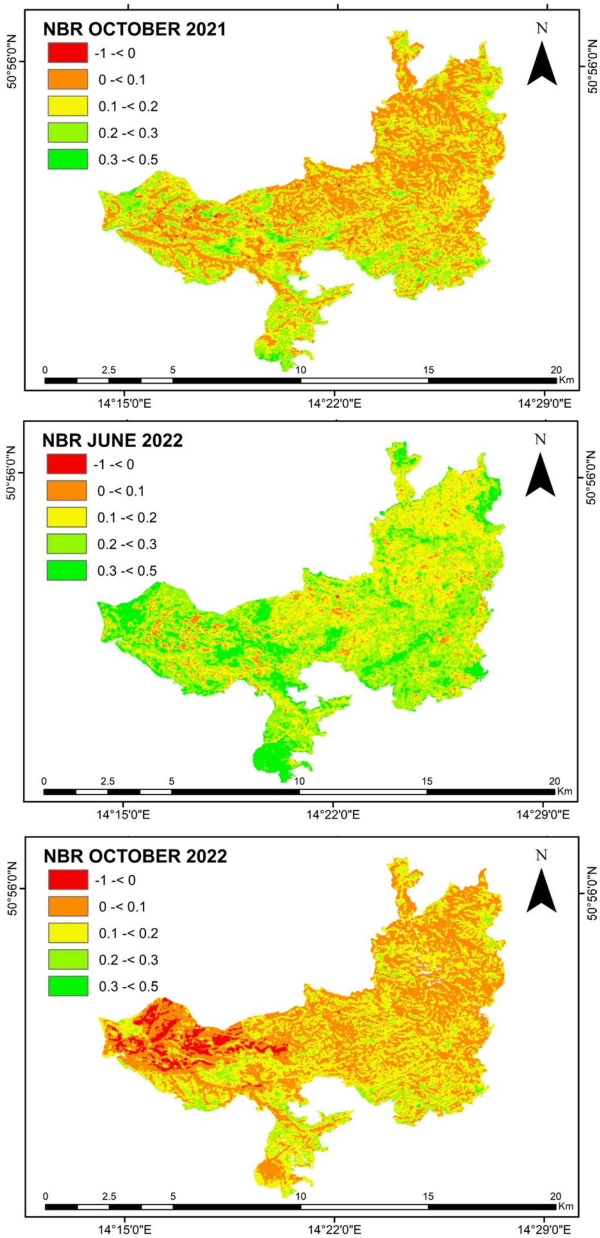

Fig. 7 NBR maps before (October 2021 and June 2022) and after the fire (October 2022) in the national park

effects of the fire are observed. NBR values are observed lower in October 2022 than other two dates in the study area. The spatial distribution NBR values were in accordance with the NDMI and NDVI values for the locality.

According to the maps of the LST and SMI values shown in Fig. 8, the highest LST values were found before the fire in June due to the summer season. LST values were evaluated for October 2021 and October 2022, and the temperature was shown to be higher in October 2022 than in October 2021. The soil moisture content was lower in October 2022 than in October 2021. According to LST and SMI maps, it is determined that as the temperature increases in the national park, the humidity decreases. According to the average LST values, after the fire, the temperature in the national park in October 2022 increased by 2.5 °C compared to October 2021. Accordingly, average SMI decreased from 0.88 to 0.79 on the same dates.

The burned area was estimated using the difference of NDVI and NBR indices in 2021 and 2022 and the approximate area is 13.20 km^2 that represents 17% of the national park.

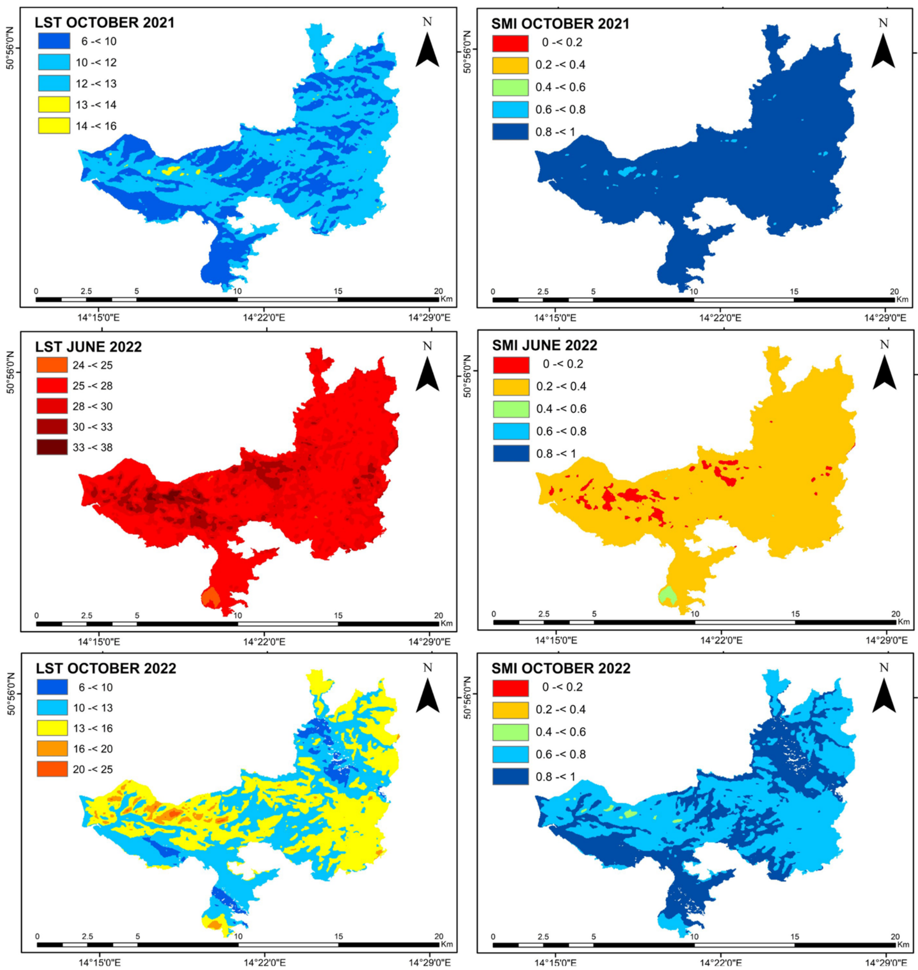

Fig. 8 Land surface temperature (°C) and soil moisture maps of the study area

The Bohemian Switzerland National Park belongs to the Natura2000 sites. According to the report of Joint Research Centre of European Commission (San-Miguel-Ayanz et al. 2023), the burned area was 14.38 km^2. The total burned area in protected areas in 2022 was the highest amount mapped in the last 10 years, 3324 individual fires (>30 ha) spread over more than 3650 km^2. Average size of one fire was about 1.1 km^2. However spatial resolution of the satellite sensor data used for that study from the MODIS sensor was 250 m, while the present study used 30 m spatial resolution (Sentinel-2).

The accuracy assessment of Landsat-8 LST values for three different images and their overall accuracy compared to MODIS are shown in Fig. 9 as scatterplots. Accuracy assessments were found with 32 homogenous pixel points in the study area. Based on the accuracy analysis of the LST data, a highly proportional relationship is observed between the Landsat-8 LST and MODIS daily LST data, with an overall coefficient of determination (r^2) of 0.92. The lowest root mean square deviation (RMSD) is identified as 1.57 °C for the three dates in October 2021, while the highest RMSD is recorded as 3.07 °C in June 2022. The overall RMSD of the LST is determined to be 2.33 °C.

The correlational relationships of SMI, NDMI and LST with NDVI were assessed based on the values calculated for 32 spatial points that are homogeneously distributed. The relationships of the indices are shown in Fig. 10; in addition they are listed in Table 1. While the strongest correlation between NDMI and NDVI is seen in the summer season as *r* value of 0.84, on the other hand, the strongest correlation between SMI and NDVI is observed in the autumn of 2021 as *r* value of -0.63. The relationship of SMI and NDMI with NDVI is found to be weaker in October 2022 after the fire, compared to October 2021. NDVI and LST relationship is stronger in October 2021 than October 2022.

While the high vegetation cover in June 2022 ensures high NDMI values, high surface temperatures in the same month reduces the moisture content in the soil. It is observed that NDMI and SMI values decrease after the fire in the autumn months of both years, while NDMI increases, and SMI decreases in the summer months.

The SMI and NDMI relationships between the two years and different seasons are shown in Fig. 11. SMI represents moisture content of the soil while NDMI is related to water content of the plant canopy. A positive correlational relationship between the soil moisture content and the vegetation water content was observed in autumn season for both years while a week correlational relationship was found during the summer in June 2022 (see Table 1).

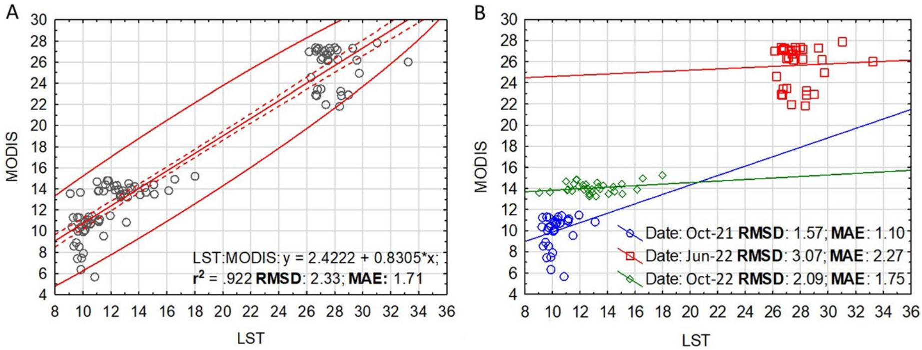

Fig. 9 Accuracy assessment of Landsat and MODIS land surface temperature; the overall accuracy assessment is on the right side (**A**) and the date specific accuracy assessment is on the left side (**B**)

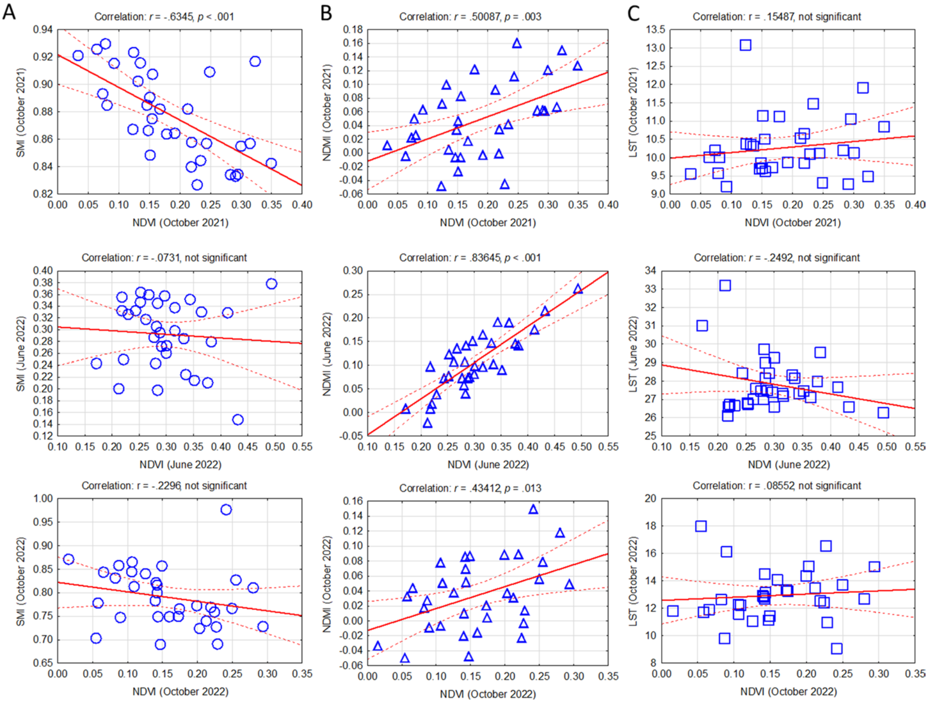

Fig. 10 Relationship between NDVI and SMI (**A**), NDMI (**B**) and LST (**C**)

Table 1 Correlation matrix of the remote sensing indices

Season	Correlation coefficient	NDVI	NDMI
October 2021	NDMI	0.5009	
June 2022	NDMI	0.8365	
October 2022	NDMI	0.4341	
October 2021	LST	0.1549	
June 2022	LST	-0.2492	
October 2022	LST	0.0855	
October 2021	SMI	-0.6345	0.1301
June 2022	SMI	-0.0731	0.3169
October 2022	SMI	-0.2296	0.4835

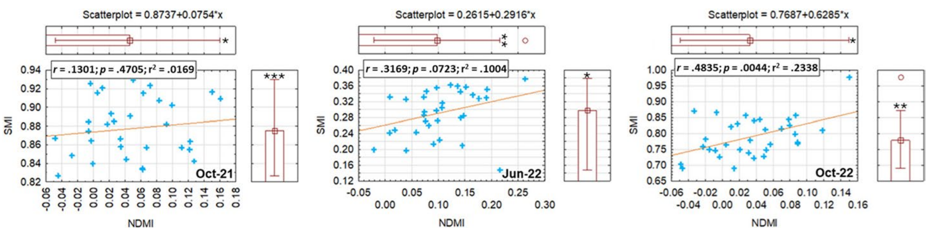

Fig. 11 Relationship between NDMI and SMI across different periods; different numbers of asterisks indicate different homogeneous groups for SMI and NDMI values separately (a higher number represents a higher mean value), according to Duncan's multiple range test ($p < 0.05$)

The fire was considerably influential on the relationship between SMI and NDMI. Briefly, the most significant positive correlation between SMI and NDMI values was observed several months after the fire in October 2022, while during the same period, SMI values were significantly lower compared to those observed in October 2021.

The NO_2 values, indicating its ratio in the atmosphere, are depicted in Fig. 12, with the unit of measurement expressed in mol/m^2. The NO_2 concentration in the atmosphere, which serves as a crucial parameter for assessing pollution levels, was observed to exhibit a significant increase immediately following the fire in the main study area.

4 Discussion

The impacts of the forest fire were examined using remote sensing indices in the Bohemian Switzerland National Park in the Czech Republic. Vegetation changes in the study area were detected using NDVI that shows density of vegetation cover while NBR is calculated to estimate burned areas. Changes in the vegetation water content and the soil moisture content after forest fire were observed using the NDMI and SMI indices. NO_2 concentration was estimated in the air of adjacent regions before fire and after the fire in the interval of approximately one month.

The averages of all index values are given in Table 2 that show the changes in land surface temperature, vegetation ratio and moisture ratio in soil and vegetation cover after the fire. According to the mean values in the Table 2, remote sensing indices have lower average value after the fire in October 2022, as it was also evident in the Figs. 6, 7 and 8.

The minimum value of NBR decreased from −0.04 to -0.18 between October 2021 and October 2022 while the maximum value is approximately similar for both years, 0.38 to 0.37, respectively. Thus, changes of NBR for the same month in different years demonstrated that index showed burned areas successfully. In a forest fire study by Çolak and Sunar (2022, 2023) were calculated NDVI and NBR indices to estimate and detect burned areas using Landsat-8 data, revealing temporal changes between pre and post fire and the study showed that NBR index values were lower after the fire than before.

LST values showed negative correlation with NDVI in June 2022 while a weak positive correlation was observed in October 2021 and October 2022 due to effect of climate con-

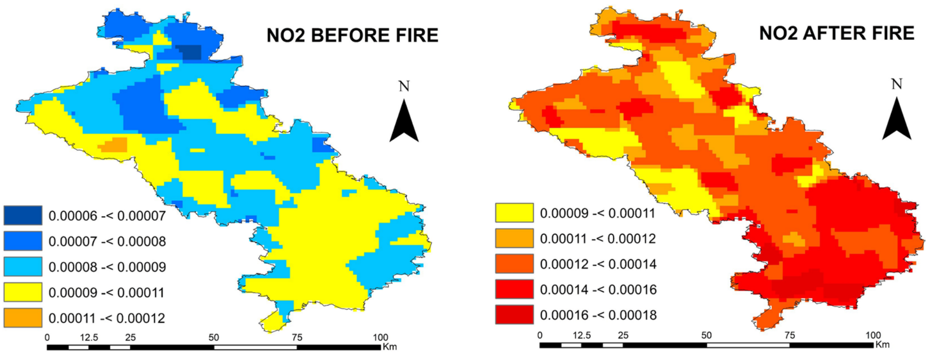

Fig. 12 Nitrogen dioxide (mol/m^2) maps of the main study area using Sentinel-5P satellite data before (between July 19th and July 21st, 2022), and after the fire (between August 21st to 23rd, 2022)

Table 2 Mean values of the remote sensing indices and MODIS daily LST

DATE	NDVI	NDMI	SMI	LST (LANDSAT-8)	LST (MODIS)
OCTOBER 2021	0.19	0.05	0.88	10.3 °C	10.0 °C
JUNE 2022	0.31	0.11	0.30	27.9 °C	25.4 °C
OCTOBER 2022	0.16	0.03	0.79	12.9 °C	14.0 °C

ditions on temperature and decreasing vegetation density at the end of vegetation season. While there was a positive correlation between LST and NDVI in the autumn period, a negative correlation was observed in the summer period, as it was observed in the study by Marzban et al. (2018). Accuracy assessment of LST values with MODIS daily LST in Fig. 9 demonstrated that overall correlation was strong ($r^2=0.92$) with RMSD = 2.33 °C. The related studies about accuracy assessment of Landsat LST with MODIS demonstrated that the RMSD range was 2.5–4.3 °C (Hengl et al. 2012; Vlassova et al. 2014; Choi et al. 2021; Yilğan et al. 2022). MODIS daily LST can have approximately 1 °C accuracy in clear weather conditions which means atmospheric transmittance and water vapour ratio of the atmosphere are analysed and integrated to the calculation phase. Thus, accuracy assessment shows that RMSD values remained in the confidence interval despite the total atmospheric effects are not eliminated in this study.

After the fire, the results demonstrated that the moisture rate in the vegetation cover and soil decreased as expected in October 2022 more than in October 2021. SMI values were the lowest during the summer in June 2022 due to high surface temperature in the study area, which is in accordance with the study performed by Hruška et al. (2022). In their analysis of SMI for March and April 2022, a severe drought was observed in the study area, which helped to create the fire risk conditions. In the present study, SMI had weaker relationship with NDVI after the fire in October 2022 ($r = -0.23$) than in October 2021 ($r = -0.63$), which can be partly explained by temperature effect of the fire. In Fig. 8 can be seen hot places in the north-west part of the national park (October 2022), which corresponds with the epicentre of the fire. However the main reason of this relationship can be explained with lower vegetation density due to burned areas.

While a positive relationship is observed between NDVI and NDMI for every season, the same relationship is not observed with SMI and NDVI because SMI is calculated using LST data and the seasonal difference in the dataset affects the relationship between SMI and NDVI. There was also a positive correlation observed between NDVI and NDMI ($r=0.74$) in the study of Strashok et al. (2022). NDMI and NDVI had a weak correlational relationship ($r=0.43$) after the fire in October 2022. NDMI and SMI had also weak positive relationships for all seasons but SMI values were lower than NDMI values after the forest fire in October 2022.

According to Fig. 12, the range of NO_2 concentration in the air doubled from 6 to 10.10^{-5} mol/m^2 to 11–17.10^{-5} mol/m^2 after the forest fire in the main study area; that means the most affected adjacent districts. The WHO annual average limit is 40 µg/m^3 as interim target, however the recommendation is as low as 10 µg/m^3 and the highest obtained value of 18.10^{-5} mol/m^2 can be converted approximately to 34.45 µg/m^3 using the WHO provided conversion factor 1.914 (WHO 2021). It should be noted, that the observation time was about 10 days after ceasing the fire. It is proven that NO_2 gas can move to distant areas during and after the fire due to climatic conditions and show an intense accumulation (e.g.

Magro et al. 2021). The smoke from this particular catastrophic fire could be sensed even in capital city of Prague about 85 km far, as authors of the present study confirm. In addition, according to Cichowicz et al. (2017), the rate of NO_2 held in the air is higher in winter than in summer. However, in this study, air quality data are not affected by a large seasonal temperature change, because Sentinel 5P satellite provides the opportunity to calculate data immediately after a fire, as it has high temporal resolution. Hruška et al. (2022) proved in their study that the cause of the rapid and uncontrollable spread of the fire in the first days was mainly high wind speed in combination with very low humidity of the soil, air, vegetation and also high temperature.

5 Conclusion

The environmental changes and their effects on vegetation, soil moisture, and air quality due to the biggest forest fire in recent decades in the Czech Republic, which happened in the Bohemian Switzerland National Park in July 2022, were investigated using satellite images by the GEE cloud-based platform. Only publicly available data were used. Several remote sensing indices such as NDVI, NDMI, LST, SMI and NBR were calculated and meaningful statistical relationships between indices were determined. The forest fire affected all observed indices in the area of the national park. In addition, air quality in the districts adjacent to the prevailing wind direction was observed and expressed as changes in the NO_2 concentration in the atmosphere. About 10 days after the fire extinguishing the concentration was doubled compared to the situation before the fire.

As an important outcome of this experimental research, it was concluded that the burned area (approximately 13.20 km^2) due to the forest fire was estimated properly, easily and rapidly using remote sensing tools. The achieved results are in accordance with the official studies. Result maps of indices showed burned areas in the study area after the fire and this information could be used for any external GIS analysis for the local authorities, governmental units as well as decision and policy makers. Also, average values of the indices clearly demonstrated that vegetation density, soil moisture and plant moisture were lower after the fire while surface temperature three months after the fire was higher than in the same time a year before (October 2021).

Author contributions All authors contributed to the study conception and design of the paper. Furkan Yilgan prepared remote sensing datasets, analysed data, calculate remote sensing indices by Google Earth Engine and wrote the first draft of the manuscript as well as prepared figures of maps of remote sensing indices. Marketa Mihalikova helped to provide ideas and grasped the overall structure of the article; Recep Serdar Kara provided ideas and did the relevant statistic calculations in the paper and prepared figures of statistics results. Mustafa Ustuner helped for the interpretation of the results and improved the manuscript. All authors read and approved the final manuscript.

Funding This work was supported by the Student Grant Project of the Faculty of Agrobiology, Food and Natural Resources No. SV23-23-21380.

Data availability All data generated or used during the study appear in the submitted article.

Declarations

Conflict of interest The authors have no relevant financial or non-financial interests to disclose.

References

Adams C, McLinden CA, Shephard MW, Dickson N, Dammers E, Chen J, Makar P, Cady-Pereira KE, Tam N, Kharol SK, Lamsal LN, Krotkov NA (2019) Satellite-derived emissions of carbon monoxide, ammonia, and nitrogen dioxide from the 2016 Horse River wildfire in the Fort McMurray area. Atmos Chem Phys 19(4):2577–2599

Al-Ghussain L (2019) Global warming: review on driving forces and mitigation. Environ Prog Sustain Energy 38(1):13–21

Bentchakal M, Medjerab A, Chibane B, Rahmani SEA (2022) Meteorological drought and remote sensing data: an approach to assess fire risks in the Algerian forest. Model Earth Syst Environ 8(3):3847–3858

Bo M, Mercalli L, Pognant F, Berro DC, Clerico M (2020) Urban air pollution, climate change and wildfires: the case study of an extended forest fire episode in northern Italy favoured by drought and warm weather conditions. Energy Rep 6:781–786

Choi S, Lee K-S, Seo M, Seong N-H, Jin D, Jung D, Sim S, Jung IG, Han K-S (2021) Comparison of Land Surface temperature algorithm using Landsat-8 data for South Korea. Korean J Remote Sens 37(1):153–160

Chung M, Jung M, Kim Y (2019) Wildfire damage assessment using multi-temporal Sentinel-2 data. Int Archives Photogrammetry Remote Sens Spat Inform Sci 42:97–102

Cichowicz R, Wielgosiński G, Fetter W (2017) Dispersion of atmospheric air pollution in summer and winter season. Environ Monit Assess 189(12):1–10

Çolak E, Sunar F (2022) Investigating the usefulness of satellite-retrieved land surface temperature (LST) in pre-and post-fire spatial analysis. Earth Sci Inf, 1–19

Çolak E, Sunar F (2023) Investigating the usefulness of satellite-retrieved land surface temperature (LST) in pre-and post-fire spatial analysis. Earth Sci Inf 16(1):945–963

Dash P, Göttsche F-M, Olesen F-S, Fischer H (2002) Land surface temperature and emissivity estimation from passive sensor data: theory and practice-current trends. Int J Remote Sens 23(13):2563–2594

De Jesus CSL, Delgado RC, Wanderley HS, Teodoro PE, Pereira MG, Lima M, de Ávila Rodrigues R, da Silva Junior CA (2022) Fire risk associated with landscape changes, climatic events and remote sensing in the Atlantic Forest using ARIMA model. Remote Sens Applications: Soc Environ 26:100761

Depountis N, Michalopoulou M, Kavoura K, Nikolakopoulos K, Sabatakakis N (2020) Estimating soil erosion rate changes in areas affected by wildfires. ISPRS Int J Geo-Inf 9(10):562

Gorelick N, Hancher M, Dixon M, Ilyushchenko S, Thau D, Moore R (2017) Google Earth Engine: planetary-scale geospatial analysis for everyone. Remote Sens Environ 202:18–27

Guildner LA, Edsinger RE (1973) The thermodynamic Kelvin temperature scale from 273.15 K to 415 K. Journal of Research of the National Bureau of Standards. Section A. Phys Chem 77(4):383

Hengl T, Heuvelink G, Perčec Tadić M, Pebesma EJ (2012) Spatio-temporal prediction of daily temperatures using time-series of MODIS LST images. Theoret Appl Climatol 107(1):265–277

Hruška J et al (2022) What factors influenced the origin and spread of the fire in České Švýcarsko National Park? Published by the Czech Ministry of Environment (in Czech). Accessed online in March 2023 from https://www.mzp.cz/cz/pozar_ceske_svycarsko_faktory

Ihlen V (2019) Landsat 8 data users handbook. US Geological Survey, Sioux Falls, SD, USA, p 55

Ishtiaque A, Nazem NI (2017) Household-level disaster-induced losses and rural–urban migration: experience from world's one of the most disaster-affected countries. Nat Hazards 86:315–326

Keeley JE, Fotheringham CJ (1997) Trace gas emissions and smoke-induced seed germination. Science 276(5316):1248–1250

Kudláčková L, Poděbradská M, Bláhová M, Cienciala E, Beranová J, McHugh C, Trnka M (2024) Using FlamMap to assess wildfire behavior in bohemian Switzerland National Park. Nat Hazards 120(4):3943–3977

Kula E, Jankovská Z (2013) Forest fires and their causes in the Czech Republic (1992–2004). J For Sci 59(2):41–53

Lambin EF, Goyvaerts K, Petit C (2003) Remotely-sensed indicators of burning efficiency of Savannah and forest fires. Int J Remote Sens 24(15):3105–3118

Leighton P (2012) Photochemistry of air pollution. Elsevier

Lohmander P (2022) Rational control of global warming dynamics via the CO_2 level, emission reductions and forestry expansion. Biomed J Sci Tech Res 47:38449–38468
Magro C, Nunes L, Gonçalves OC, Neng NR, Nogueira JMF, Rego FC, Vieira P (2021) Atmospheric trends of CO and CH4 from extreme wildfires in Portugal using Sentinel-5P TROPOMI level-2 data. Fire 4(2):25
Mansoor S, Farooq I, Kachroo MM, Mahmoud AED, Fawzy M, Popescu SM, Alyemeni MN, Sonne C, Rinklebe J, Ahmad P (2022) Elevation in wildfire frequencies with respect to the climate change. J Environ Manage 301:113769
Marzban F, Sodoudi S, Preusker R (2018) The influence of land-cover type on the relationship between NDVI–LST and LST-T air. Int J Remote Sens 39(5):1377–1398
McLauchlan KK, Higuera PE, Miesel J, Rogers BM, Schweitzer J, Shuman JK, Watts AC (2020) Fire as a fundamental ecological process: research advances and frontiers. J Ecol 108(5):2047–2069
Medvedkov A, Vysotskaya A, Olchev A (2023) Detection of Geocryological conditions in Boreal Landscapes of the Southern Cryolithozone using Thermal Infrared Remote Sensing Data: a case study of the Northern Part of the Yenisei Ridge. Remote Sens 15(2):291
Naqvi HR, Mutreja G, Shakeel A, Singh K, Abbas K, Naqvi DF, Chaudhary AA, Siddiqui MA, Gautam AS, Gautam S, Naqvi AR (2023) Wildfire-induced pollution and its short-term impact on COVID-19 cases and mortality in California. Gondwana Res 114:30–39
Parida BR, Collado WB, Borah R, Hazarika MK, Samarakoon L (2008) Detecting drought-prone areas of rice agriculture using a MODIS-derived soil moisture index. GIScience Remote Sens 45(1):109–129
Rabiei-Dastjerdi H, Mohammadi S, Saber M, Amini S, McArdle G (2022) Spatiotemporal analysis of NO2 Production using TROPOMI Time-Series images and Google Earth Engine in a Middle Eastern Country. Remote Sens 14(7):1725
San-Miguel-Ayanz J, Durrant T, Boca R, Maianti P, Liberta` G, Vivancos A, Felix Oom TJ, Branco D, De Rigo A, Ferrari D, Pfeiffer D, Grecchi H, Onida R, Loffler M (2022) P. Forest Fires in Europe, Middle East and North Africa 2021, EUR 31269 EN, Publications Office of the European Union, Luxembourg, ISBN 978-92-76-58585-5, https://doi.org/10.2760/34094, JRC130846
San-Miguel-Ayanz J, Durrant T, Boca R, Maianti P, Libertá G, Oom D, Branco A, de Rigo D, Ferrari D, Roglia E, Scionti N (2023) Advance report on Forest Fires in Europe, Middle East and North Africa 2022. Publications Office of the European Union, Luxembourg. https://doi.org/10.2760/091540,JRC133215
Sannigrahi S, Pilla F, Basu B, Basu AS, Sarkar K, Chakraborti S, Joshi PK, Zhang Q, Wang Y, Bhatt S (2020) Examining the effects of forest fire on terrestrial carbon emission and ecosystem production in India using remote sensing approaches. Sci Total Environ 725:138331
Siachalou S, Doxani G, Tsakiri-Strati M (2009) Integrating remote sensing processing and GIS to fire risk zone mapping: a case study for the Seih-Sou forest of Thessaloniki. Proceeding of ICC
Skalák P, Farda A, Zahradníček P, Trnka M, Hlásny T, Štěpánek P (2018) Projected shift of Köppen–Geiger zones in the central Europe: a first insight into the implications for ecosystems and the society. Int J Climatol 38(9):3595–3606
Smith AMS, Wooster MJ, Drake NA, Dipotso FM, Falkowski MJ, Hudak AT (2005) Testing the potential of multi-spectral remote sensing for retrospectively estimating fire severity in African savannahs. Remote Sens Environ 97(1):92–115
Sobrino JA, Raissouni N (2000) Toward remote sensing methods for land cover dynamic monitoring: application to Morocco. Int J Remote Sens 21(2):353–366
Sobrino JA, Caselles V, Becker F (1990) Significance of the remotely sensed thermal infrared measurements obtained over a citrus orchard. ISPRS J Photogrammetry Remote Sens 44(6):343–354
Sobrino JA, Jiménez-Muñoz JC, Paolini L (2004) Land surface temperature retrieval from LANDSAT TM 5. Remote Sens Environ 90(4):434–440. https://doi.org/10.1016/j.rse.2004.02.003
Špulák P (2022) Wildland fires in the Czech Republic—Review of data spanning 20 years. ISPRS Int J Geo-Inf 11(5):289
Strashok O, Ziemiańska M, Strashok V (2022) Evaluation and correlation of Sentinel-2 NDVI and NDMI in Kyiv (2017–2021). J Ecol Eng 23(9):212–218
Tonbul H, Kavzoglu T, Kaya S (2016) Assessment of fire severity and post-fire regeneration based on topographical features using multitemporal landsat imagery: a case study in Mersin, Turkey. Remote Sensing and Spatial Information Sciences, vol 41. International Archives of the Photogrammetry, p B8
Trochta J, Král K, Šamonil P (2012) Effects of wildfire on a pine stand in the Bohemian Switzerland National Park. J for Sci 58(7):299–307
Tucker CJ (1979) Red and photographic infrared linear combinations for monitoring vegetation. Remote Sens Environ 8(2):127–150
Vlassova L, Perez-Cabello F, Nieto H, Martín P, Riaño D, de La Riva J (2014) Assessment of methods for land surface temperature retrieval from Landsat-5 TM images applicable to multiscale tree-grass ecosystem modeling. Remote Sens 6(5):4345–4368

Walter J, Bartoňová AS, Fric ZF (2022) The impact of a forest fire event on moth assemblages in Western Bohemia, Czech Republic. Pol J Ecol 69(3–4):156–171
Weng Q, Lu D, Schubring J (2004) Estimation of land surface temperature–vegetation abundance relationship for urban heat island studies. Remote Sens Environ 89(4):467–483
World Health Organisation (2021) WHO global air quality quidelines. Particulate matter (PM2.5 and PM10), ozone, nitrogen dioxide, sulfur dioxide and carbon monoxide. Geneva. Accessed online in June 2023 from https://www.who.int/publications/i/item/9789240034228
Xiuwan C (2002) Using remote sensing and GIS to analyse land cover change and its impacts on regional sustainable development. Int J Remote Sens 23(1):107–124
Xu H (2006) Modification of normalised difference water index (NDWI) to enhance open water features in remotely sensed imagery. Int J Remote Sens 27(14):3025–3033
Yilğan F, Miháliková M, Vopravil J, Matula S, Kara RS (2022) Analysis of Soil Moisture and Temperature Regime by Using Remote Sensing in South Bohemia, Czech Republic. 2022 International Conference on Electrical, Computer and Energy Technologies (ICECET), 1–6
Yin S, Wang X, Guo M, Santoso H, Guan H (2020) The abnormal change of air quality and air pollutants induced by the forest fire in Sumatra and Borneo in 2015. Atmos Res 243(April):105027. https://doi.org/10.1016/j.atmosres.2020.105027
Yuan C, Liu Z, Zhang Y (2017) Aerial images-based forest fire detection for firefighting using optical remote sensing techniques and unmanned aerial vehicles. J Intell Robotic Syst 88(2):635–654

Authors and Affiliations

Furkan Yilgan[1] · Markéta Mihálikovál[1] · Recep Serdar Kara[1] · Mustafa Ustuner[2]

✉ Markéta Mihálikovál
mihalikova@af.czu.cz

Furkan Yilgan
yilgan@af.czu.cz

Recep Serdar Kara
karar@af.czu.cz

Mustafa Ustuner
mustuner@artvin.edu.tr

1 Department of Water Resources, Faculty of Agrobiology, Food and Natural Resources, Czech University of Life Sciences Prague, Kamýcká 129, Praha 6 165 00, Czech Republic

2 Department of Geomatics Engineering, Faculty of Engineering, Artvin Coruh University, Çayağzı, Kazım Karabekir Street, Artvin 08000, Türkiye